Electronic Supplementary Material (ESI) for Journal of Materials Chemistry C.

Electronic Supplementary Information

Two-step Phosphorescent Mechanochromism Due to Intramolecular Deformation

Xu Zhang,* Li-Yi Zhang, Jin-Yun Wang, Feng-Rong Dai and Zhong-Ning Chen*

State Key Laboratory of Structural Chemistry, Fujian Institute of Research on the Structure of Matter, Chinese Academy of Sciences, Fuzhou, Fujian 350002, China

Table S1. Crystallographic data of Pt_2Cu complex **1** with different solvate molecules.

	1·4CH_2Cl_2	**1**·3acetone	**1**·4THF
empirical formula	$C_{108}H_{99}Cl_9CuNO_4P_6Pt_2$	$C_{113}H_{109}ClCuNO_7P_6Pt_2$	$C_{120}H_{124}ClCuNO_8P_6Pt_2$
formula weight	2433.47	2268.00	2383.19
crystal system	monoclinic	triclinic	monoclinic
space group	*C*2/c	$P\bar{1}$	$P2_1/n$
a (Å)	15.370(5)	15.936(3)	15.2879(18)
b (Å)	26.440(8)	16.420(4)	25.337(3)
c (Å)	25.463(8)	21.180(4)	28.373(4)
α (deg)	90	73.227(3)	90
β (deg)	91.741(5)	84.428(6)	94.403(3)
γ (deg)	90	88.948(6)	90
V (Å^3)	10343(5)	5280.6(19)	10958(2)
Z	4	2	4
ρ_{calcd} (g/cm^{-3})	1.563	1.426	1.445
μ (mm^{-1})	3.279	3.012	2.908
radiation (λ, Å)	0.71073	0.71073	0.71073
temperature (K)	293(2)	293(2)	293(2)
completeness	99.0	99.0	99.6
GOF	1.040	1.104	1.128
R1 (F_o)[a]	0.0622	0.0464	0.0517
*w*R2 (F_o^2)[b]	0.2339	0.1389	0.1978

Table S2. Partial Molecular Orbital Compositions (%) in the Ground State for Pt_2Cu Complex **1** in the CH_2Cl_2 Solution by TD-DFT Method at the B3LYP Level.

orbital	energy	MO contribution (%)				
	(eV)	Pt (s/p/d)	Cu (s/p/d)	dpmp	decz	$C{\equiv}CC_6H_5$
LUMO+9	-1.02	14.57 (40/39/21)	3.20 (53/42/6)	52.01	22.06	8.17
LUMO+8	-1.09	8.61 (36/47/16)	2.85 (53/37/9)	58.06	26.68	3.80
LUMO+7	-1.13	15.42 (48/38/14)	1.97 (19/71/10)	76.30	2.76	3.55
LUMO+5	-1.27	23.35 (68/8/25)	6.44 (82/16/3)	58.03	5.99	6.19
LUMO+4	-1.29	8.36 (14/49/37)	1.64 (24/52/24)	83.21	2.59	4.20
LUMO+3	-1.37	20.87 (36/16/48)	6.61 (79/19/3)	63.98	5.33	3.22
LUMO+2	-1.40	11.54 (45/10/45)	2.69 (58/26/15)	78.39	2.35	5.02
LUMO+1	-1.64	24.28 (51/25/24)	6.75 (42/52/6)	57.91	3.63	7.42
LUMO	-1.87	14.07 (14/67/19)	9.13 (58/32/10)	61.22	5.84	9.74
HOMO	-5.15	5.95 (3/7/90)	0.31 (11/81/9)	5.64	87.04	1.07
HOMO-1	-5.65	17.15 (8/2/90)	4.50 (46/23/31)	4.93	48.13	25.30
HOMO-2	-5.73	16.12 (13/3/84)	10.66 (66/10/24)	7.61	36.58	29.04
HOMO-3	-5.89	22.52 (9/2/90)	18.25 (12/9/79)	11.78	10.55	36.90
HOMO-5	-6.31	27.63 (5/2/92)	13.73 (11/4/85)	13.37	28.03	17.24

Table S3. The Absorption Transitions for Pt_2Cu Complex **1** in the CH_2Cl_2 Solution by TD-DFT Method at the B3LYP Level.

state	*E*, nm (eV)	O.S.	transition (contri.)	assignment	exp. (nm)
S_1	448 (2.77)	0.0036	HOMO→LUMO (95%)	^{1}LLCT/^{1}LMCT	
S_2	409 (3.03)	0.0223	HOMO→LUMO+1 (92%)	^{1}LLCT/^{1}LMCT	405
S_3	384 (3.23)	0.0700	HOMO-1→LUMO (63%)	^{1}LLCT/^{1}MC	372
			HOMO-3→LUMO (13%)	^{1}LLCT/^{1}MC/^{1}MLCT/^{1}IL	
			HOMO→LUMO+3 (10%)	^{1}LLCT/^{1}LMCT	
S_8	364 (3.41)	0.0668	HOMO→LUMO+4 (44%)	^{1}LLCT	
			HOMO→LUMO+5 (34%)	^{1}LLCT/^{1}LMCT	
S_{10}	357 (3.48)	0.0831	HOMO-1→LUMO+1 (45%)	^{1}LLCT/^{1}MC/^{1}LMCT	356
			HOMO-2→LUMO+1 (20%)	^{1}LLCT/^{1}MC	
			HOMO-2→LUMO (10%)	^{1}LLCT/^{1}MC	
			HOMO→LUMO+5 (9%)	^{1}LLCT/^{1}LMCT	
S_{12}	349 (3.56)	0.1377	HOMO-2→LUMO+1 (35%)	^{1}LLCT/^{1}MC	
			HOMO→LUMO+9 (14%)	^{1}LLCT/^{1}IL/^{1}LMCT	
			HOMO-1→LUMO+1 (12%)	^{1}LLCT/^{1}MC/^{1}LMCT	
S_{13}	345 (3.60)	0.1938	HOMO→LUMO+8 (30%)	^{1}LLCT/^{1}IL	
			HOMO→LUMO+7 (14%)	^{1}LLCT/^{1}LMCT	
			HOMO-3→LUMO+1 (13%)	^{1}MC/^{1}LLCT/^{1}IL/^{1}MLCT	
			HOMO-2→LUMO+1 (9%)	^{1}LLCT/^{1}MC	
S_{24}	322 (3.85)	0.1376	HOMO-3→LUMO+2 (28%)	^{1}LLCT/^{1}MLCT/^{1}MC/^{1}IL	312
			HOMO-5→LUMO+1 (11%)	^{1}LLCT/^{1}MC/^{1}IL/^{1}MLCT	

Table S4. Partial Molecular Orbital Compositions (%) and Emission Transition in the Lowest Triplet State for Pt_2Cu Complex **1** in the CH_2Cl_2 Solution by TD-DFT Method at the B3LYP Level.

orbital	energy (eV)	MO contribution (%)				
		Pt (s/p/d)	Cu (s/p/d)	dpmp	decz	$C{\equiv}CC_6H_5$
LUMO	-2.44	26.44 (41/19/40)	4.75 (48/42/10)	55.03	6.69	7.09
HOMO	-4.98	7.51 (4/12/85)	0.65 (2/90/8)	4.66	85.99	1.19

state	*E*, nm (eV)	O.S.	transition (Contri.)	assignment	exp. (nm)
T_1	649 (1.91)	0.0000	HOMO→LUMO (89%)	^{3}LLCT/^{3}LMCT	672

Table S5. Partial Molecular Orbital Compositions (%) in the Lowest Triplet State for **1**·4THF, **1**·3acetone and **1**·$4CH_2Cl_2$ by TD-DFT Method at the B3LYP Level.

orbital	energy (eV)	MO contribution (%)				
		Pt (s/p/d)	Cu (s/p/d)	dpmp	decz	$C{\equiv}CC_6H_5$
			1·4THF			
LUMO	-3.20	17.99 (41/49/10)	9.87 (37/52/11)	65.55	3.78	2.81
HOMO	-6.33	6.51 (7/13/79)	0.31 (19/59/22)	5.24	86.54	1.40
			1·3acetone			
LUMO	-3.43	28.80 (57/27/16)	9.55 (21/75/4)	52.09	4.95	4.61
HOMO	-6.36	5.97 (4/15/81)	0.59 (50/44/6)	4.17	88.25	1.03
			1·$4CH_2Cl_2$			
LUMO	-3.41	10.64 (6/83/12)	12.83 (68/21/11)	70.68	4.16	1.69
HOMO	-6.21	5.18 (2/4/94)	0.25 (0/85/15)	7.28	85.94	1.35

Table S6. The Emission Transitions for **1**·4THF, **1**·3acetone and **1**·$4CH_2Cl_2$ by TD-DFT Method at the B3LYP Level.

state	*E*, nm (eV)	O.S.	transition (contri.)	assignment	exp. (nm)
1·4THF	491 (2.52)	0.0000	HOMO→LUMO (80%)	^{3}LLCT/^{3}LMCT	525
1·3acetone	518 (2.39)	0.0000	HOMO→LUMO (95%)	^{3}LLCT/^{3}LMCT	556
1·$4CH_2Cl_2$	560 (2.22)	0.0000	HOMO→LUMO (93%)	^{3}LLCT/^{3}LMCT	630

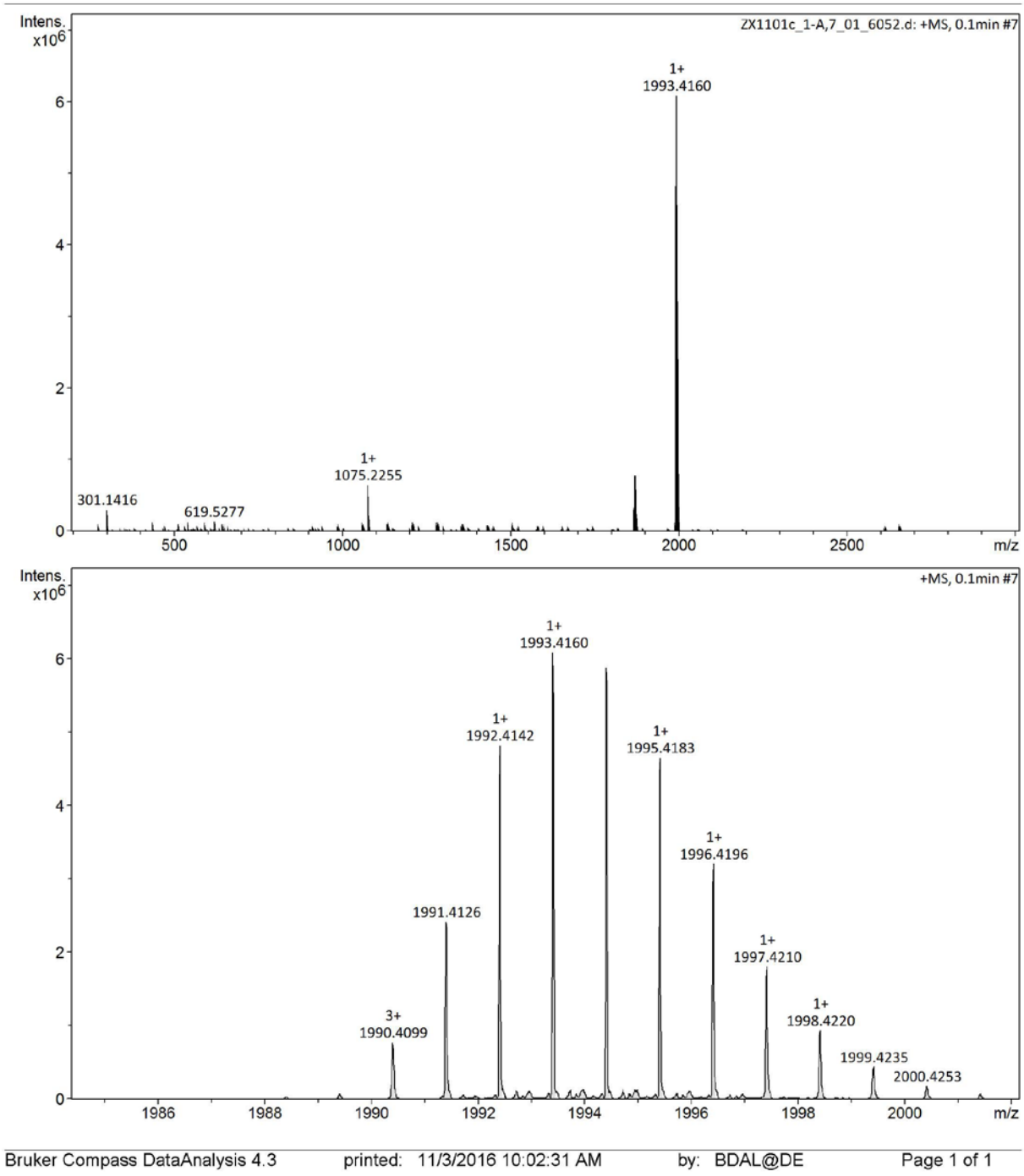

Fig. S1. High-resolution mass spectrometry of $PtCu_2$ complex **1**.

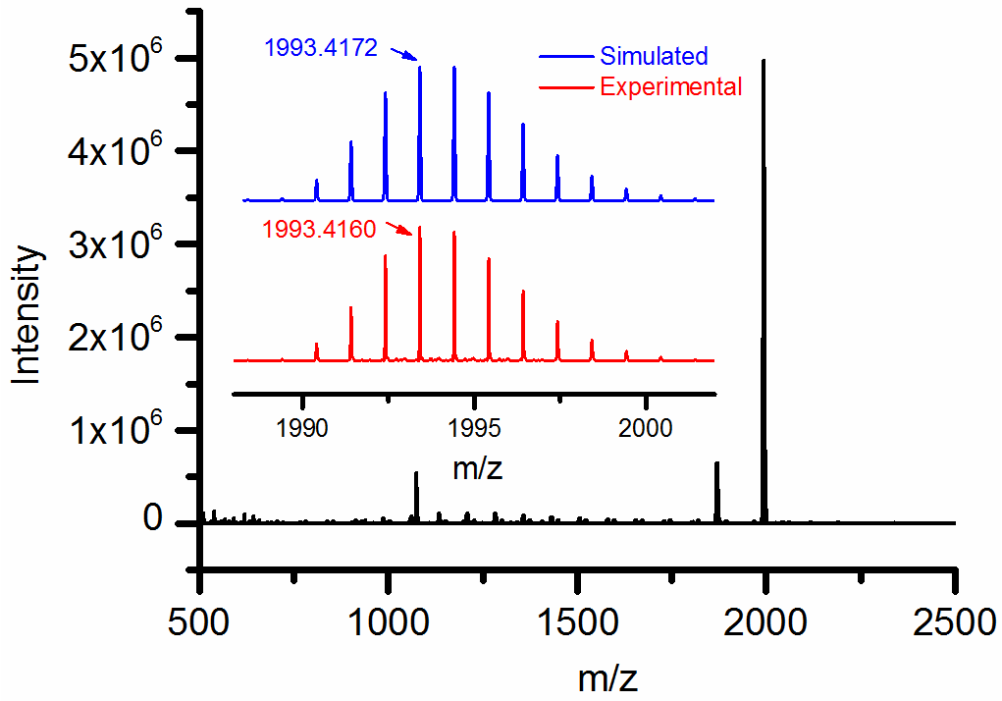

Fig. S2. High-resolution mass spectrometry of $PtCu_2$ complex **1**. Inset: The measured and simulated isotopic patterns.

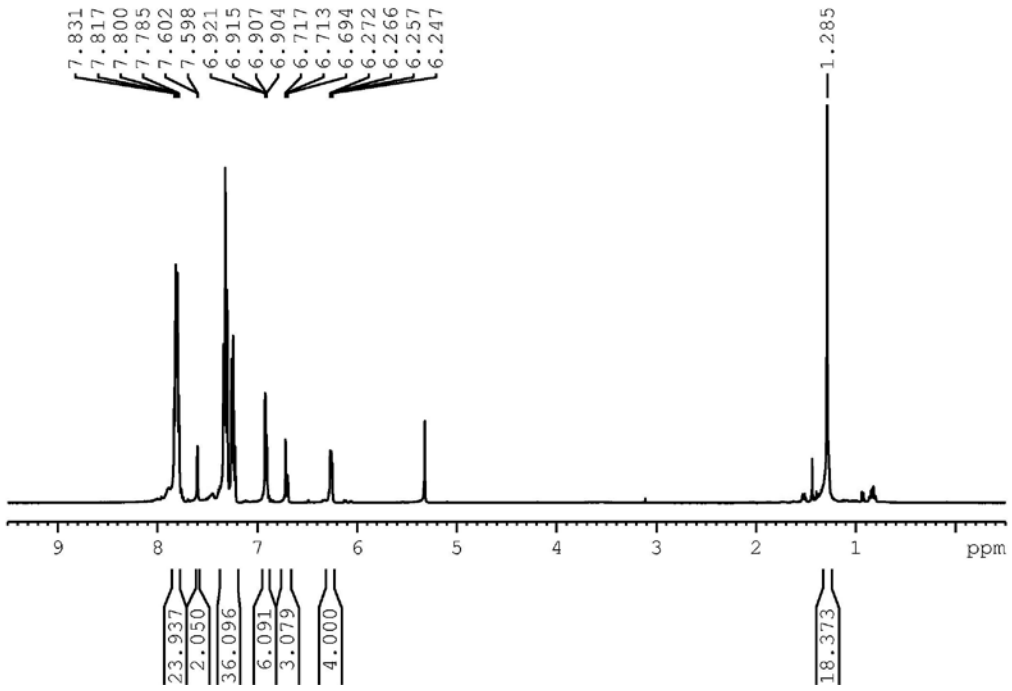

Fig. S3. The ^{1}H NMR spectrum of precursor complex $Pt_2(PPh_3)_4(\mu\text{-decz})(C{\equiv}CPh)_2$ in CD_2Cl_2 solution at ambient temperature.

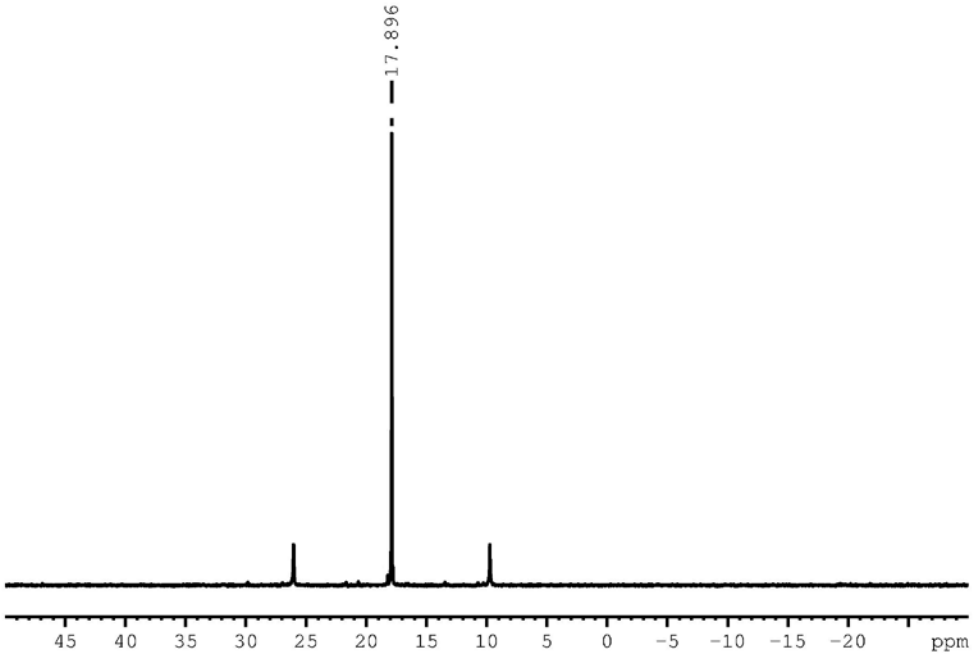

Fig. S4. The $^{31}P\{^{1}H\}$ NMR spectrum of precursor complex $Pt_2(PPh_3)_4(\mu\text{-decz})(C{\equiv}CPh)_2$ in $CDCl_3$ solution at ambient temperature.

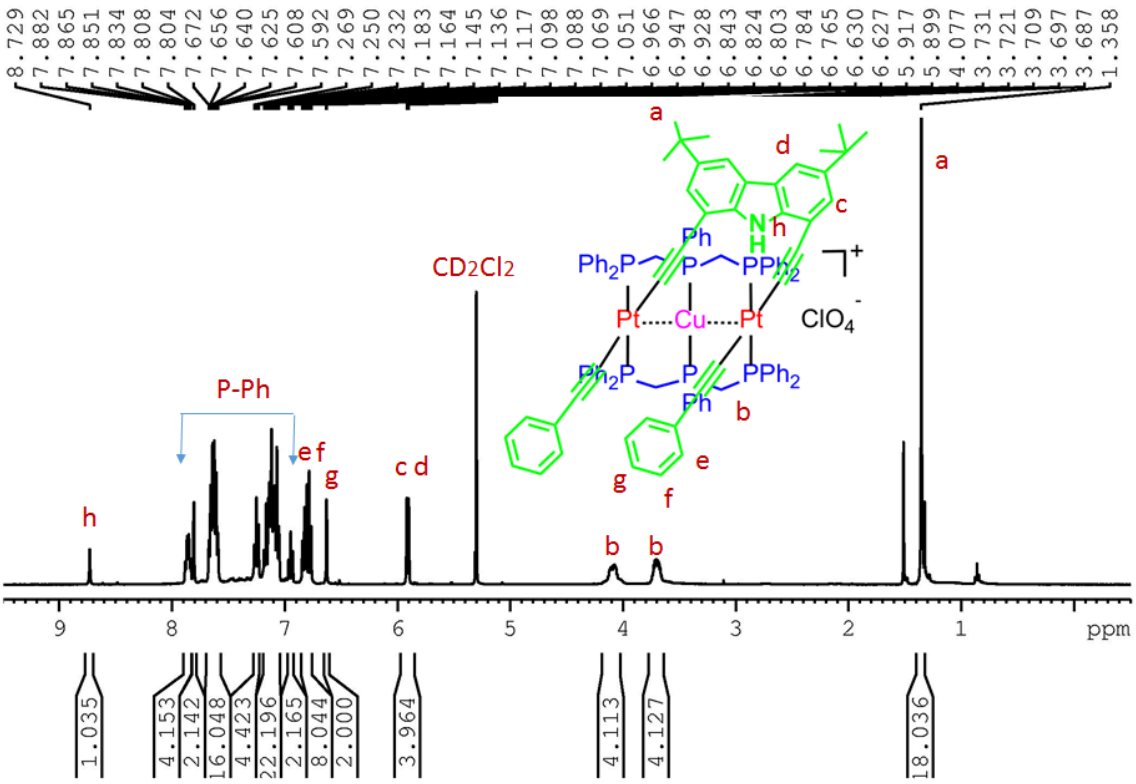

Fig. S5. The ^{1}H NMR spectrum of Pt_2Cu complex **1** in CD_2Cl_2 solution at ambient temperature.

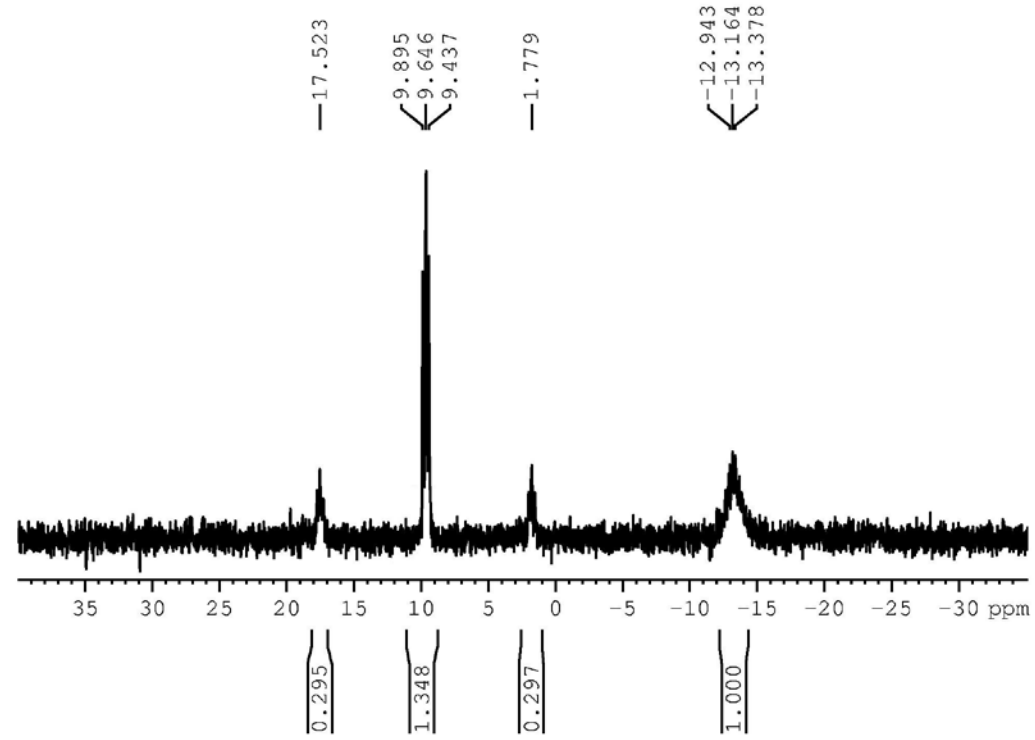

Fig. S6. The $^{31}P\{^{1}H\}$ NMR spectrum of Pt_2Cu complex **1** in CD_2Cl_2 solution at ambient temperature.

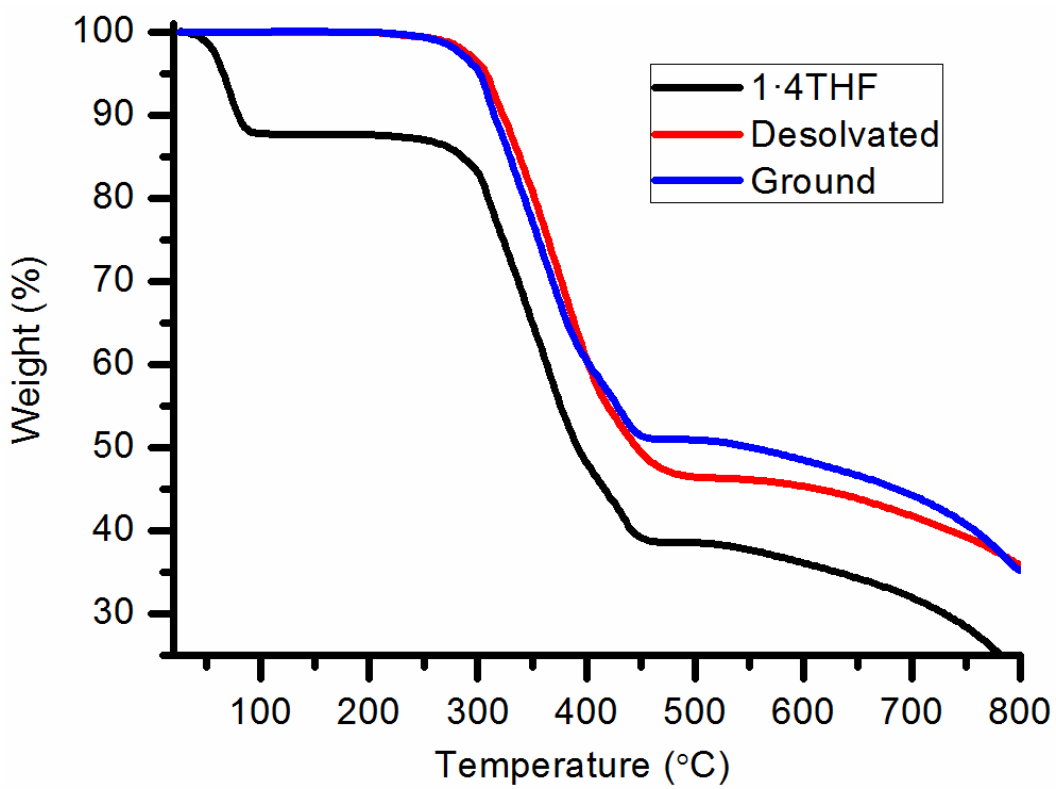

Fig. S7. The polts of thermogravimetric analyses of **1**·4THF, desolvated and ground species.

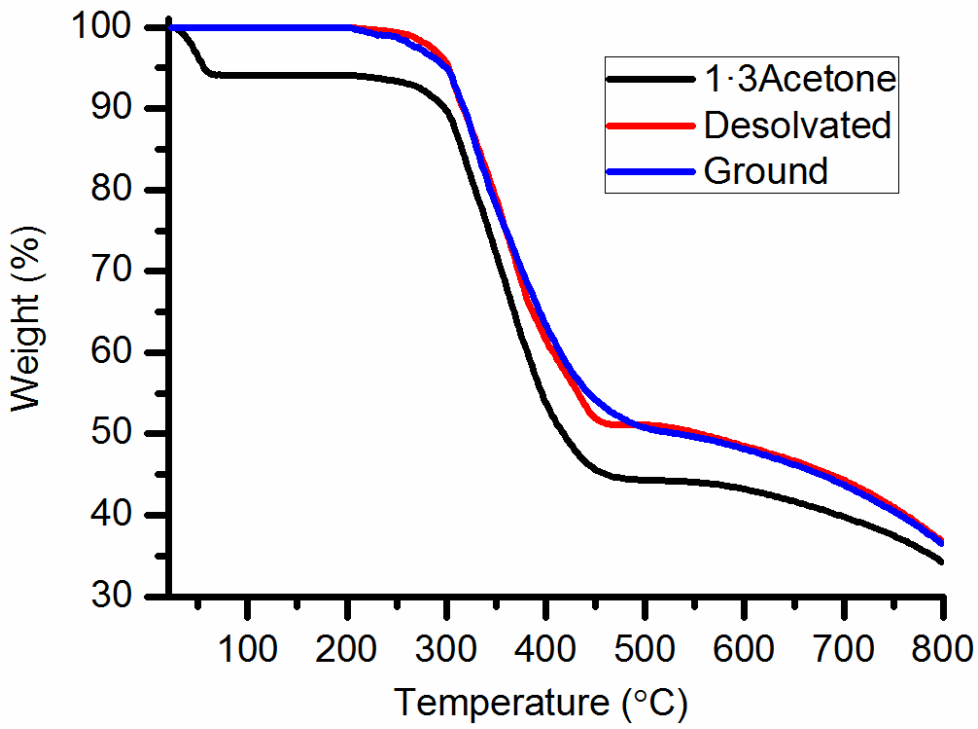

Fig. S8. The polts of thermogravimetric analyses of **1**·3acetone, desolvated and ground species.

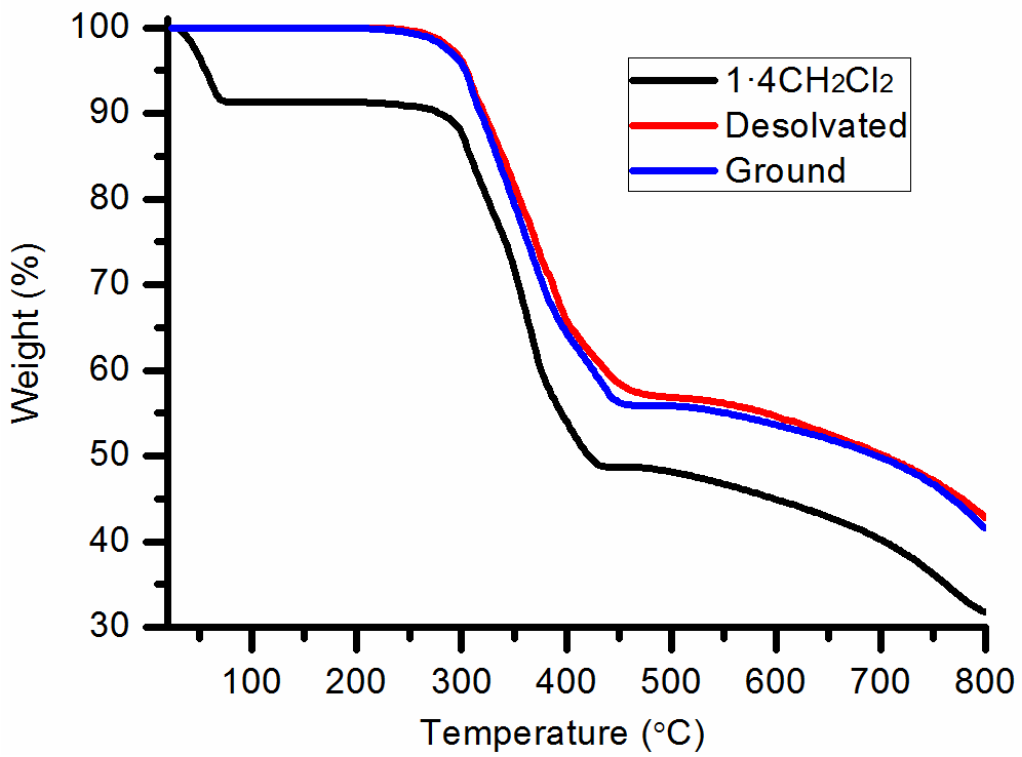

Fig. S9. The polts of thermogravimetric analyses of **1**·4CH_2Cl_2, desolvated and ground species.

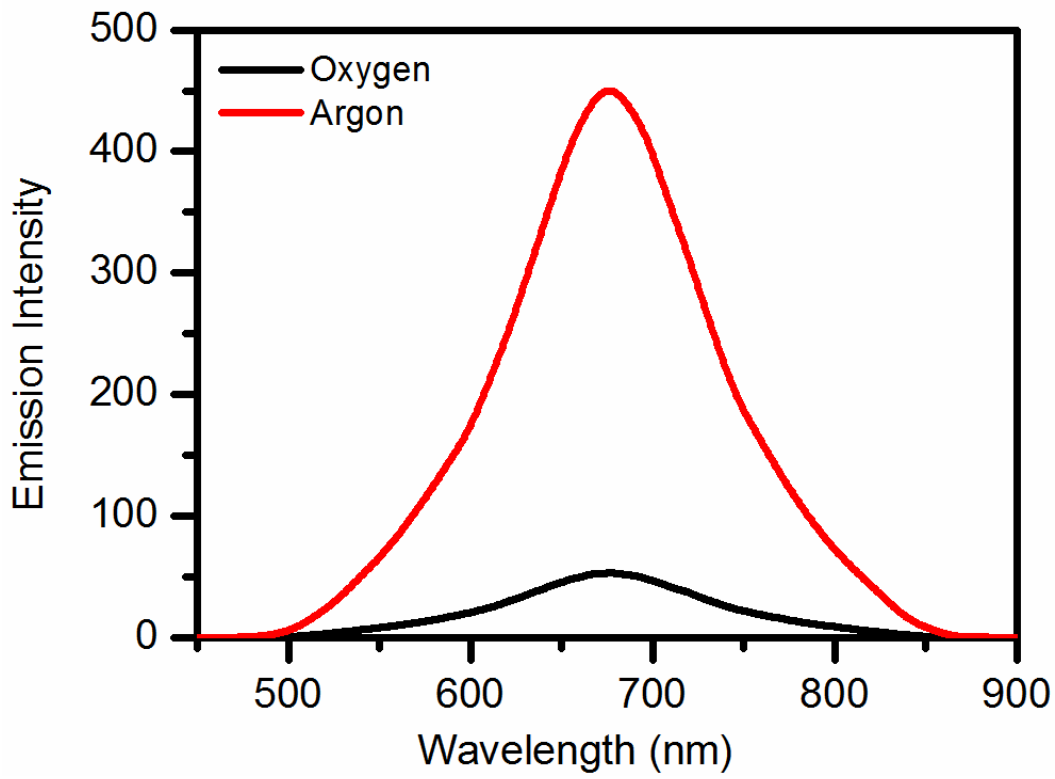

Fig. S10. The emission spectra of complex **1** in argon-bubbled and oxygen-bubbled CH_2Cl_2 solution.

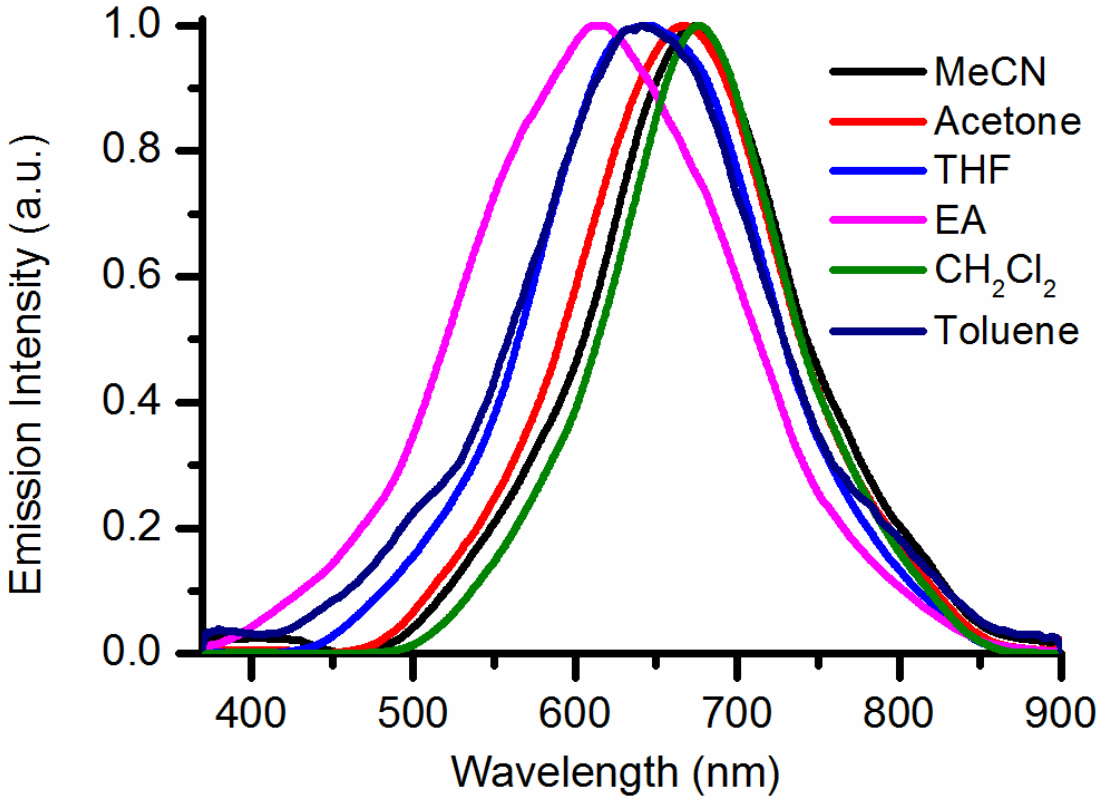

Fig. S11. The emission spectra of complex **1** in various solvent solution.

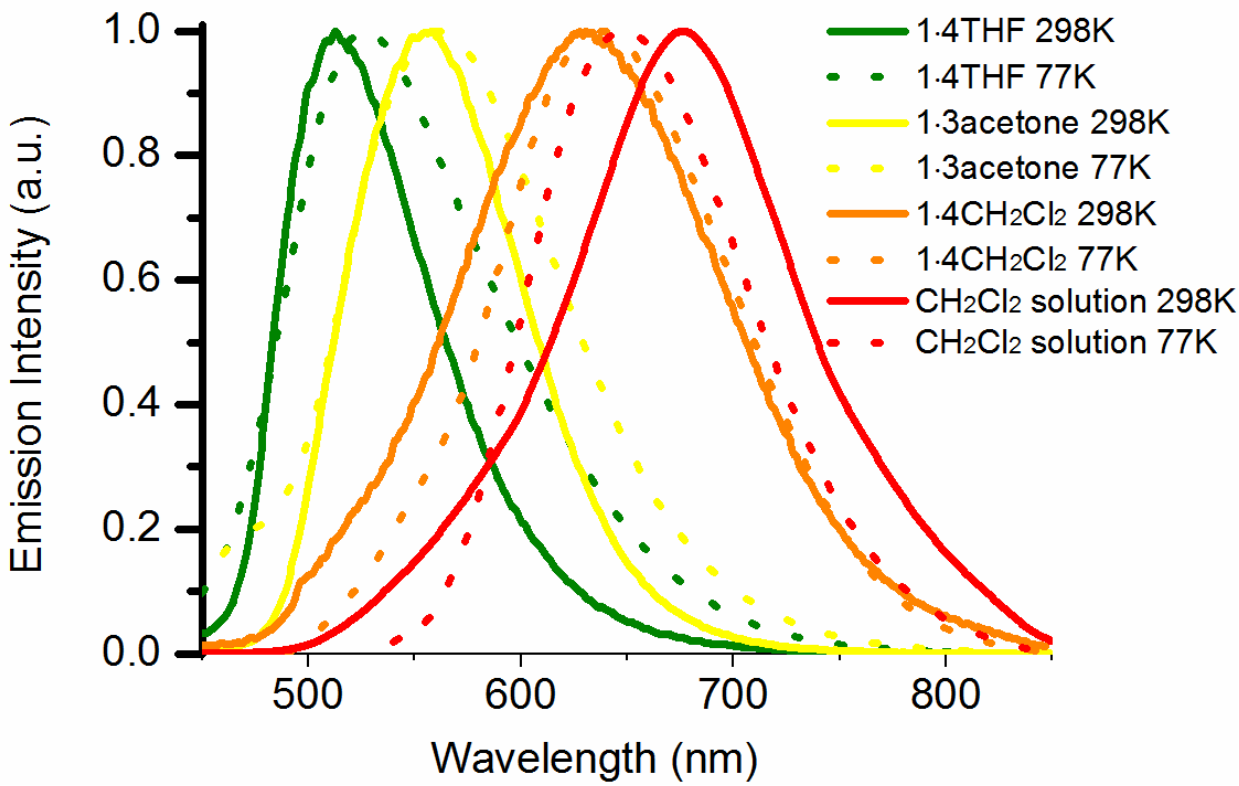

Fig. S12. The emission spectra of complex **1** in various states at 298K and 77K.

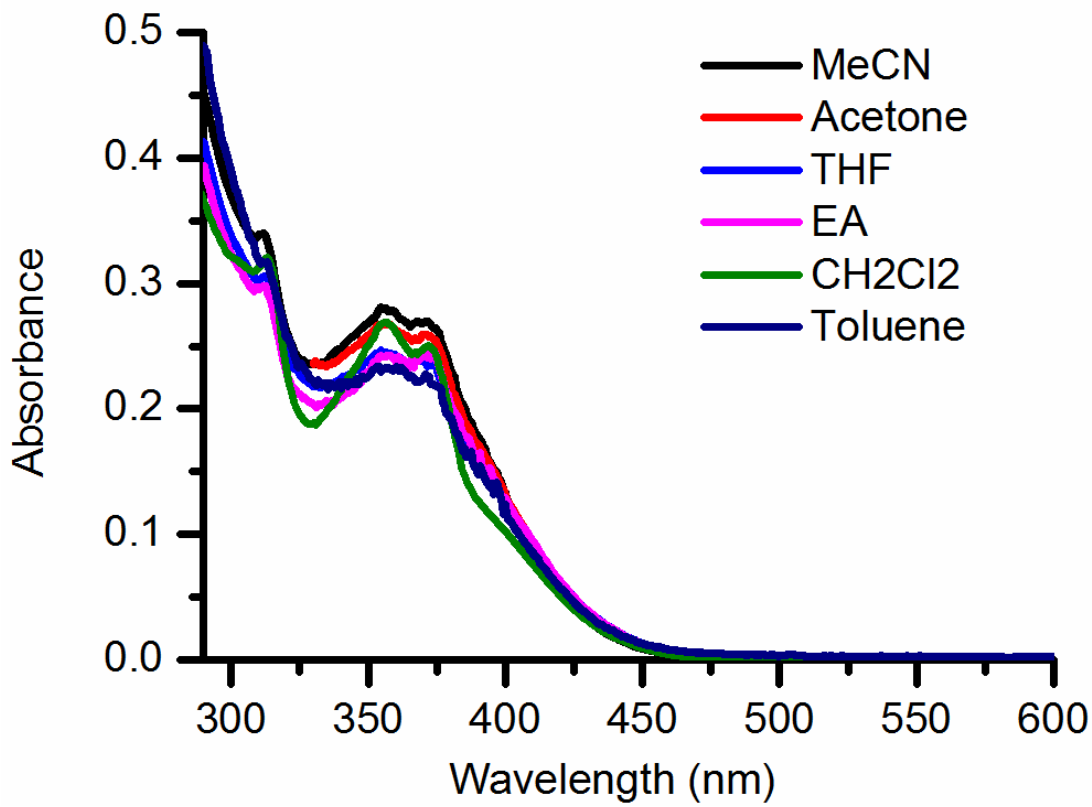

Fig. S13. UV−vis spectra of complex **1** in various solvent solution at 298K.

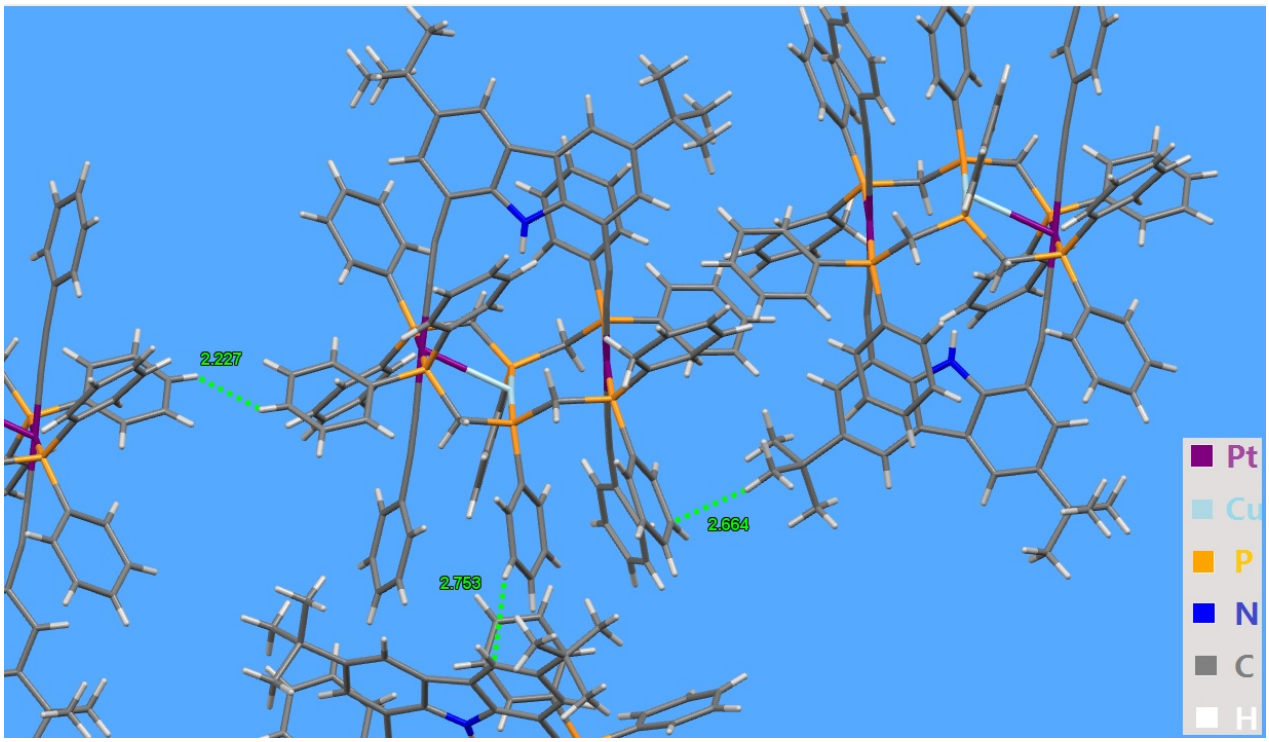

Fig. S14. Plot of molecular stacking in **1**·4THF, showing weak intermolecular contacts.

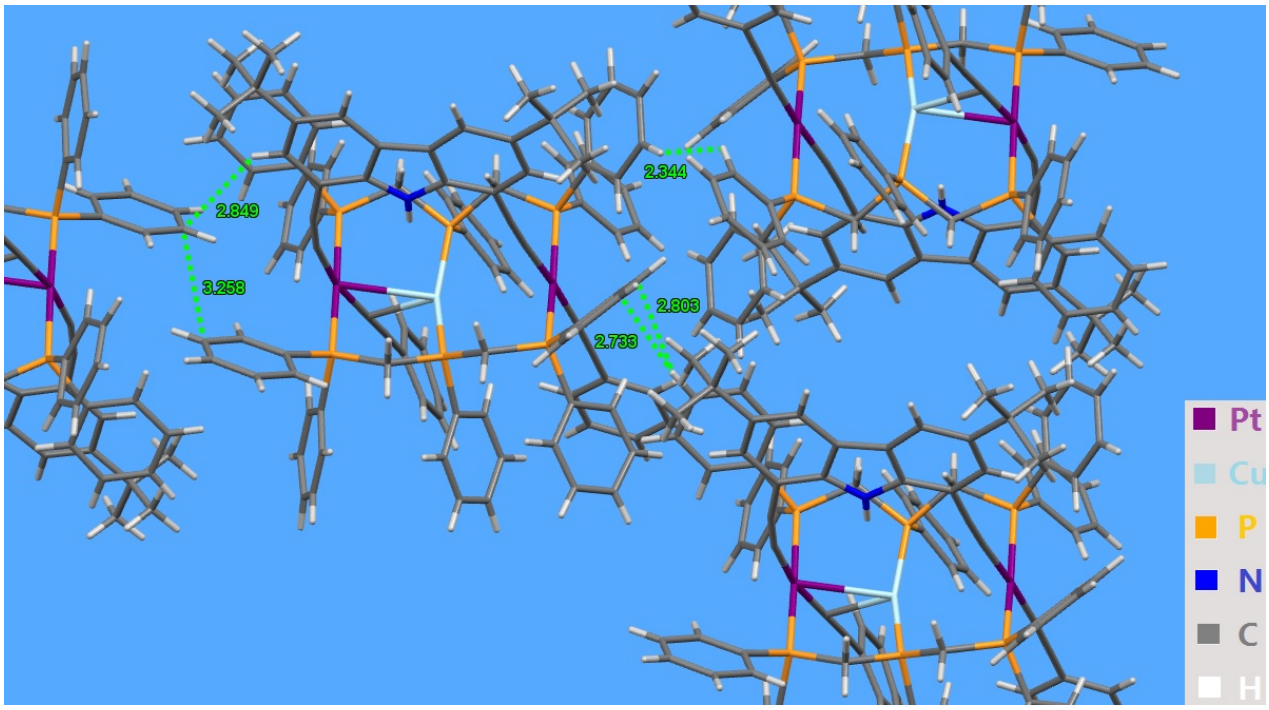

Fig. S15. Plot of molecular stacking in **1**·3acetone, showing weak intermolecular contacts.

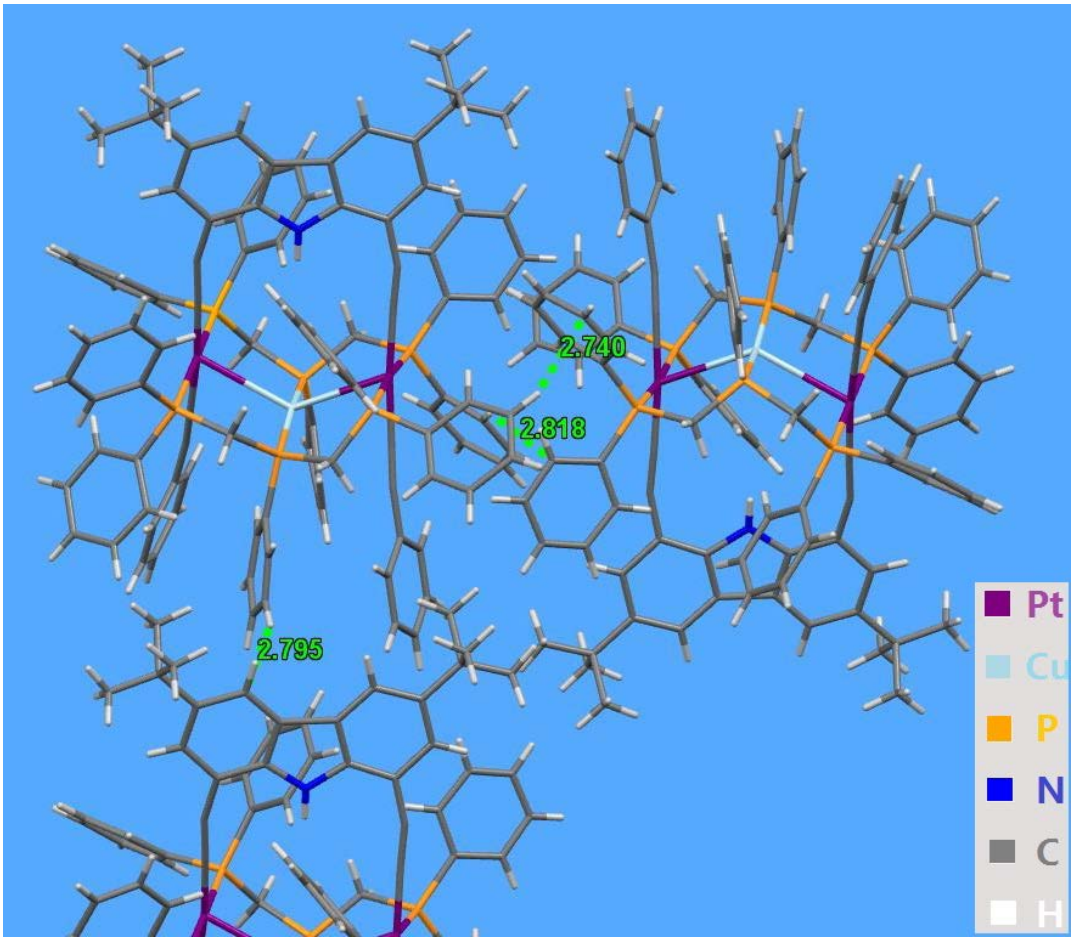

Fig. S16. Plot of molecular stacking in **1**·4CH_2Cl_2, showing weak intermolecular contacts.

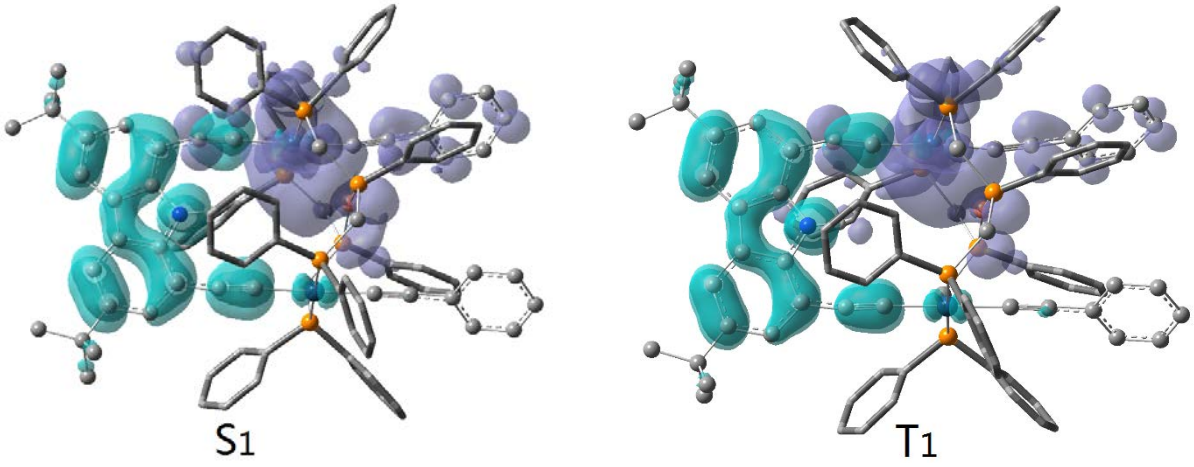

Fig. S17. The transition orbital distribution in the lowest singlet and triplet states for Pt_2Cu complex **1** in CH_2Cl_2 by TD-DFT method at the B3LYP level (isovalue = 0.0006). The blue-green represents electron depletion (ED) region, and the purple stands for electron accumulation (EA) region. For clarity, the hydrogen atoms are omitted.

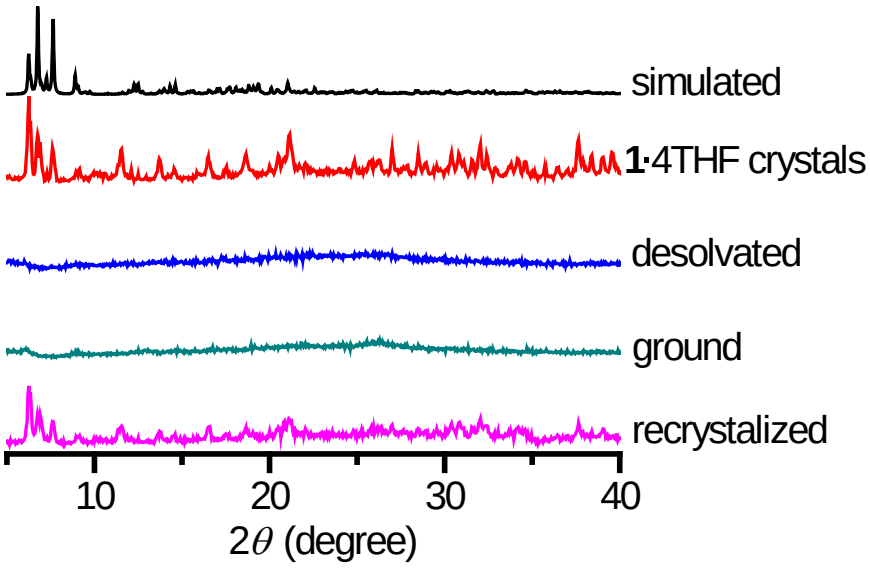

Fig. S18. The changes of X-ray diffraction (XRD) patterns for crystalline morp **1**·4THF and the corresponding desolvated species in response to mechanical grinding, showing reversible reversion to the crystalline state upon recrystallization in THF.

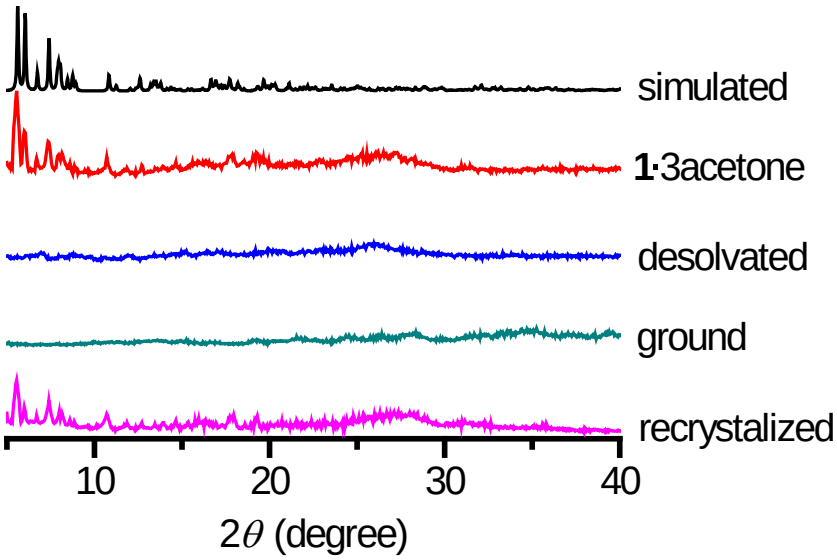

Fig. S19. The changes of X-ray diffraction (XRD) patterns for crystalline morp **1**·3acetone and the corresponding desolvated species in response to mechanical grinding, showing reversible reversion to the crystalline state upon recrystallization in acetone.

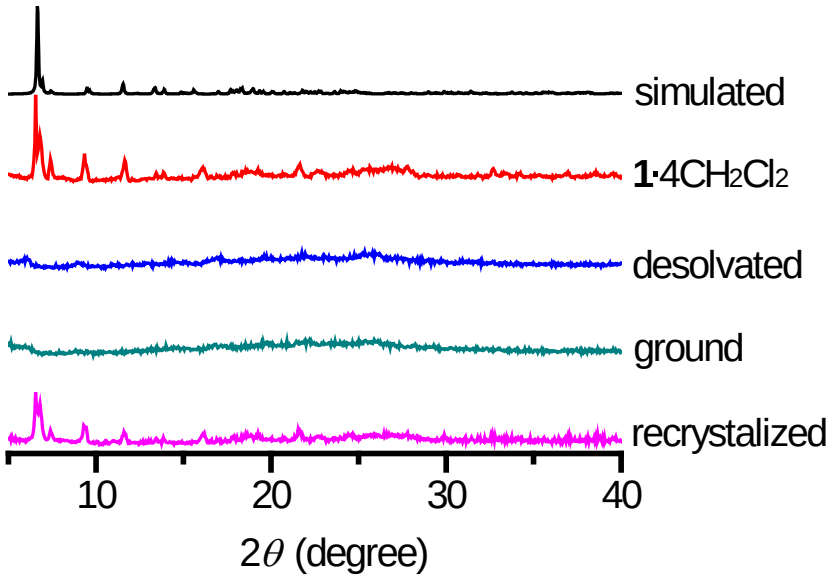

Fig. S20. The changes of X-ray diffraction (XRD) patterns for crystalline morp **1**·4CH_2Cl_2 and the corresponding desolvated species in response to mechanical grinding, showing reversible reversion to the crystalline state upon recrystallization in CH_2Cl_2.

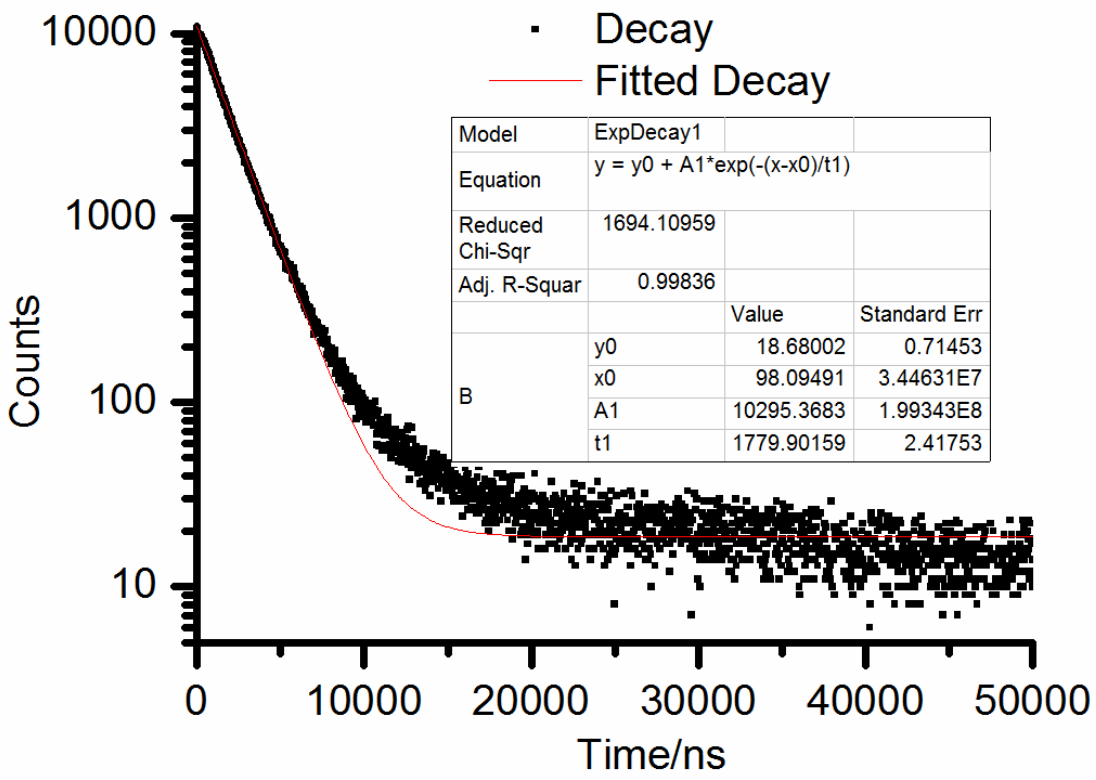

Fig. S21. The decay curve of crystal sample of **1**·4THF.

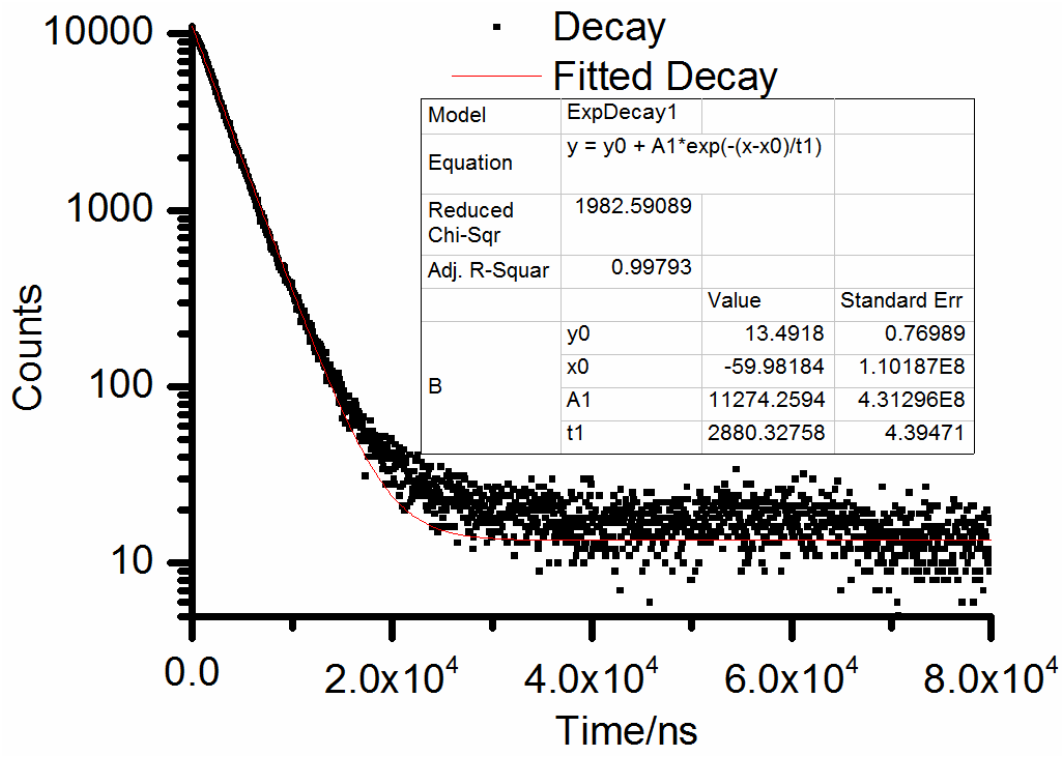

Fig. S22. The decay curve of desolvated sample of **1**·4THF.

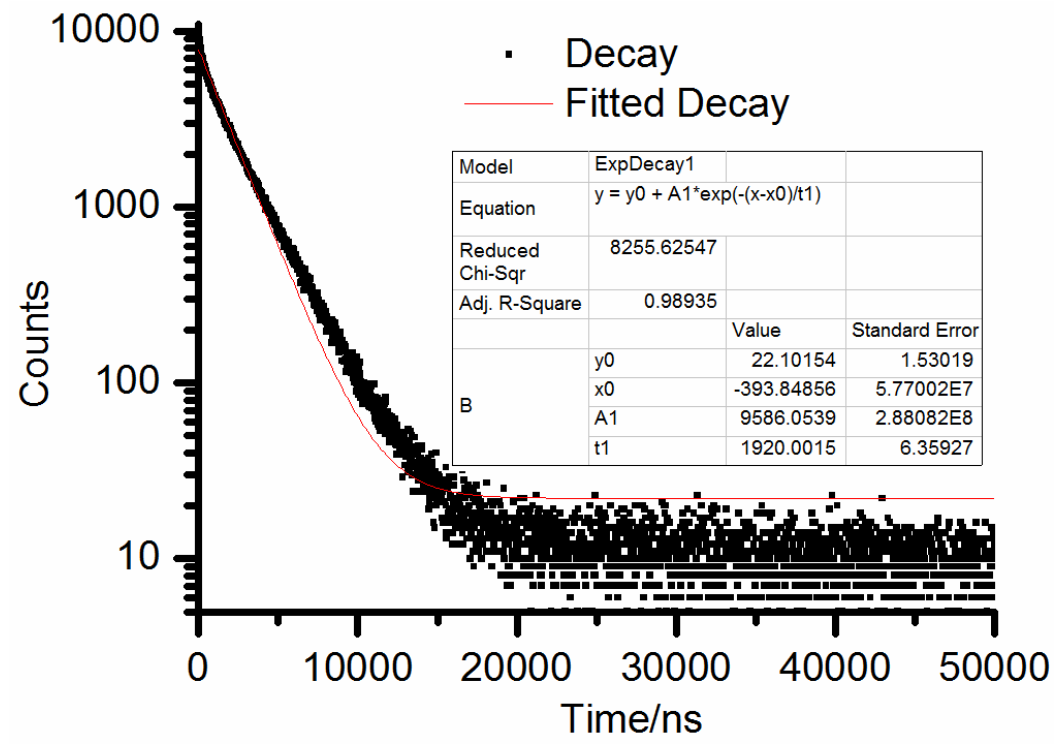

Fig. S23. The decay curve of ground sample of **1**·4THF.

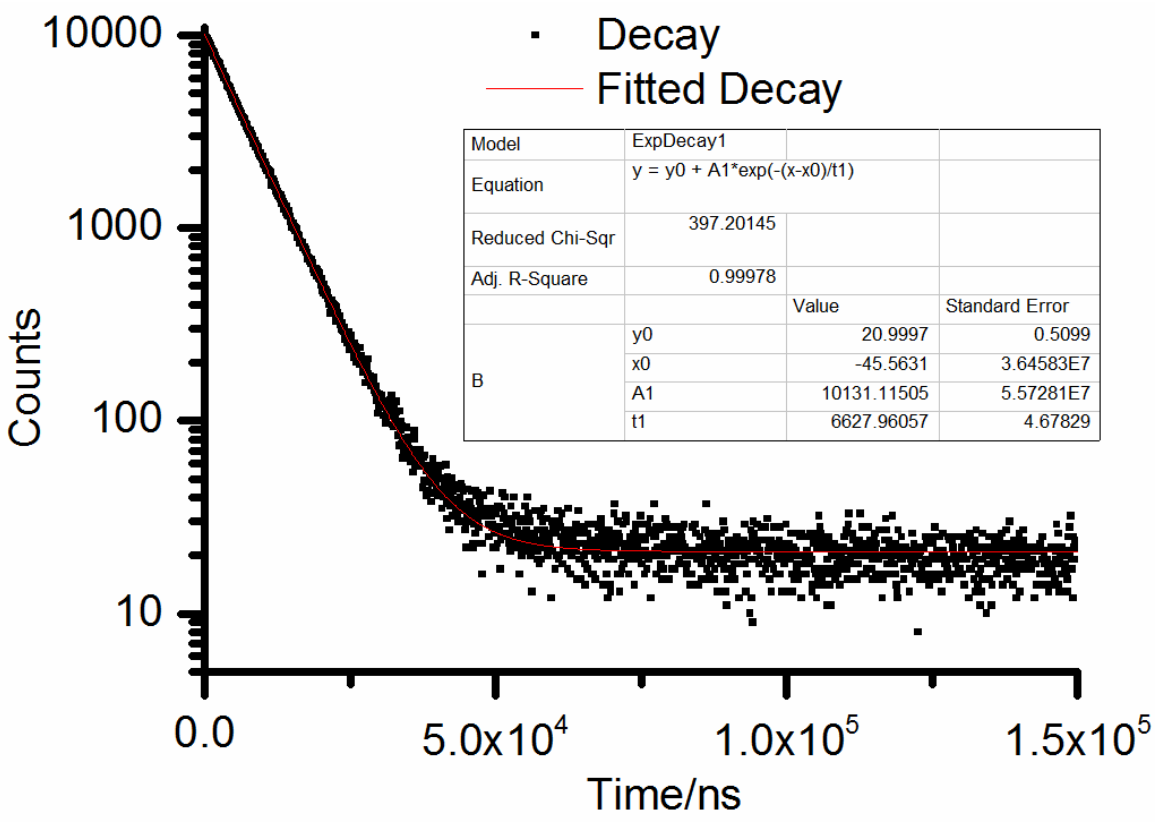

Model	ExpDecay1		
Equation	y = y0 + A1*exp(-(x-x0)/t1)		
Reduced Chi-Sqr	397.20145		
Adj. R-Square	0.99978		
		Value	Standard Error
B	y0	20.9997	0.5099
	x0	-45.5631	3.64583E7
	A1	10131.11505	5.57281E7
	t1	6627.96057	4.67829

Fig. S24. The decay curve of crystal sample of **1**·3acetone.

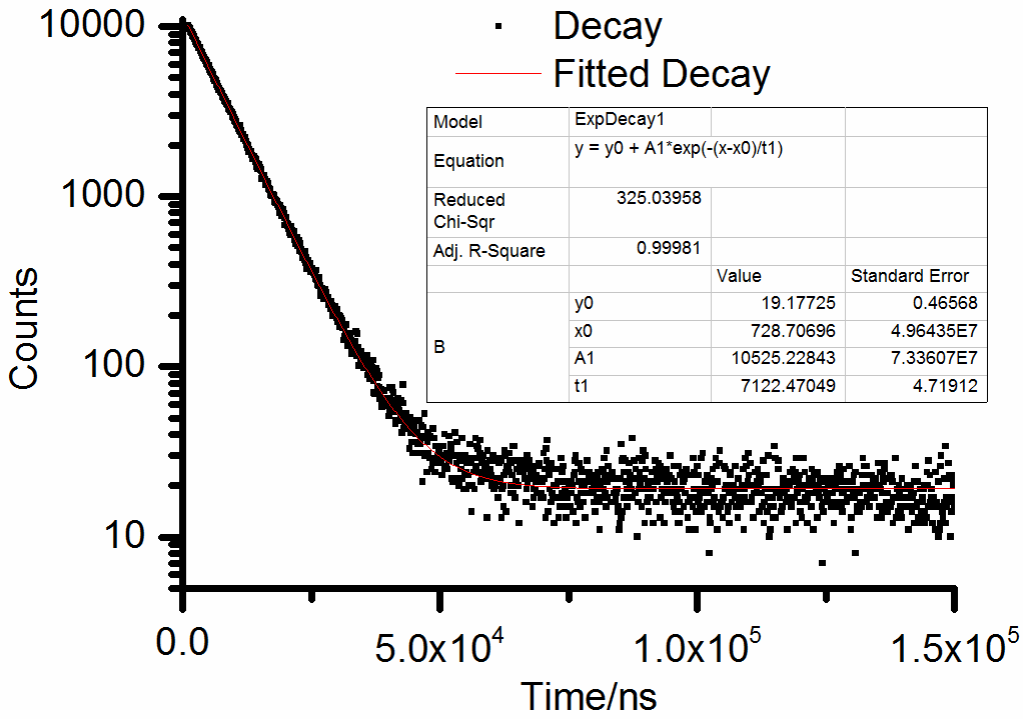

Model	ExpDecay1		
Equation	y = y0 + A1*exp(-(x-x0)/t1)		
Reduced Chi-Sqr	325.03958		
Adj. R-Square	0.99981		
		Value	Standard Error
B	y0	19.17725	0.46568
	x0	728.70696	4.96435E7
	A1	10525.22843	7.33607E7
	t1	7122.47049	4.71912

Fig. S25. The decay curve of desolvated sample of **1**·3acetone.

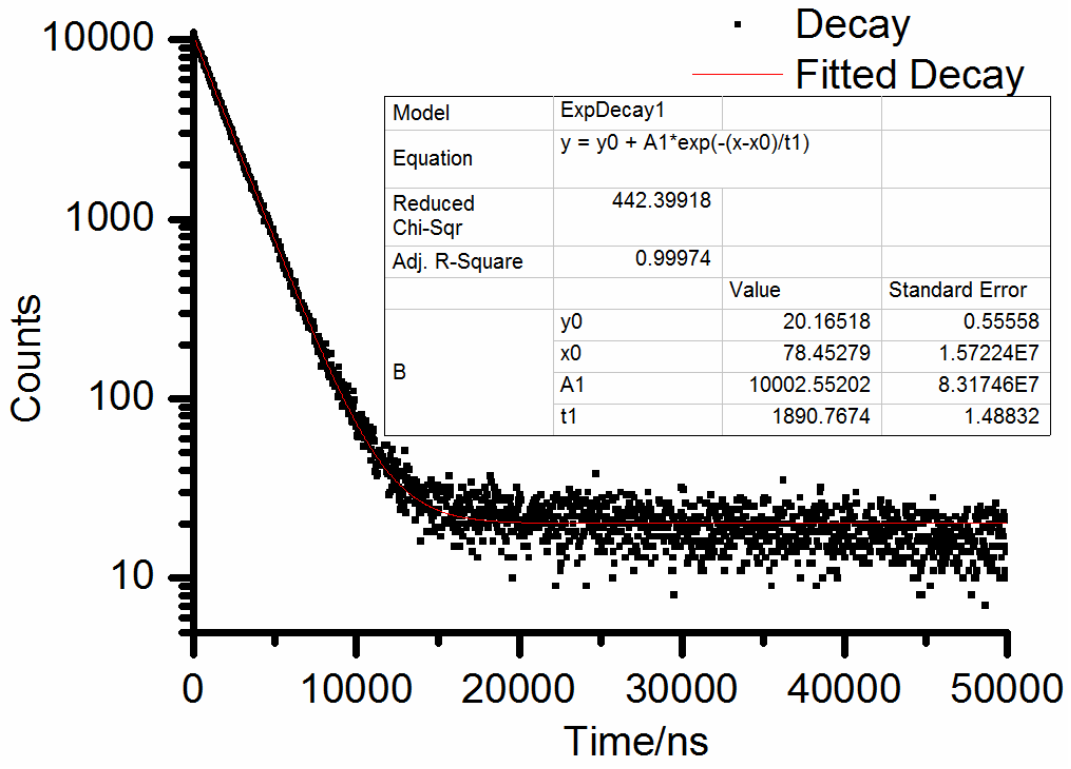

Fig. S26. The decay curve of ground sample of **1**·3acetone.

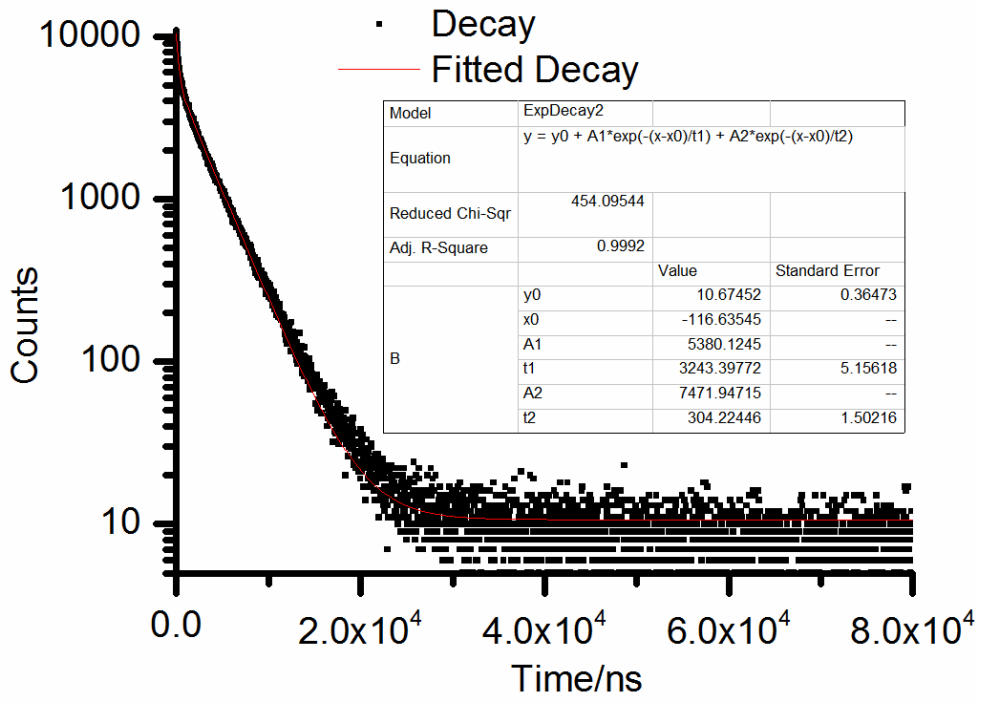

Fig. S27. The decay curve of crystal sample of **1**·4CH_2Cl_2.

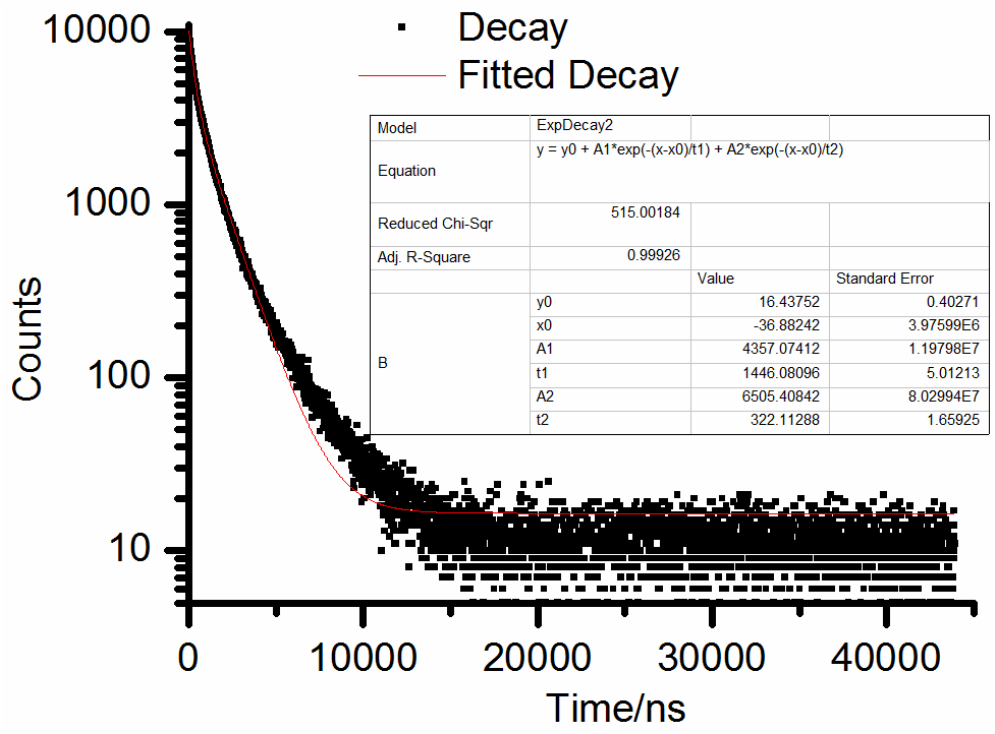

Model	ExpDecay2		
Equation	y = y0 + A1*exp(-(x-x0)/t1) + A2*exp(-(x-x0)/t2)		
Reduced Chi-Sqr	515.00184		
Adj. R-Square	0.99926		
		Value	Standard Error
B	y0	16.43752	0.40271
	x0	-36.88242	3.97599E6
	A1	4357.07412	1.19798E7
	t1	1446.08096	5.01213
	A2	6505.40842	8.02994E7
	t2	322.11288	1.65925

Fig. S28. The decay curve of desolvated sample of **1**·4CH_2Cl_2.

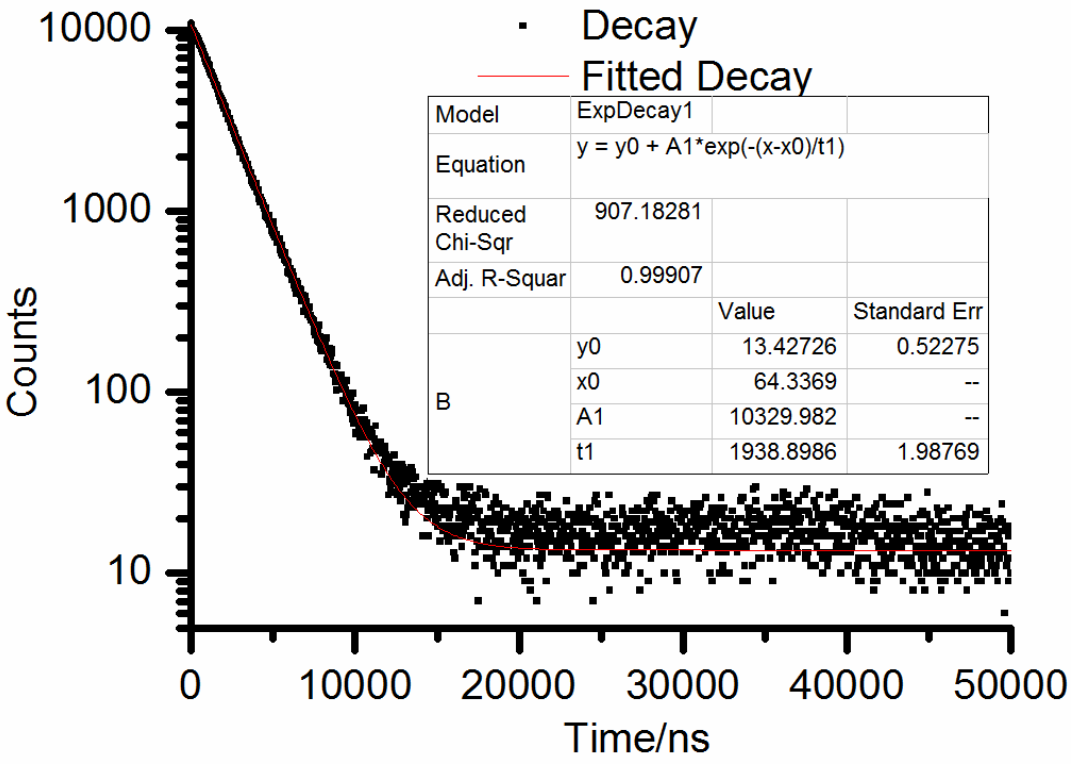

Model	ExpDecay1		
Equation	y = y0 + A1*exp(-(x-x0)/t1)		
Reduced Chi-Sqr	907.18281		
Adj. R-Squar	0.99907		
		Value	Standard Err
B	y0	13.42726	0.52275
	x0	64.3369	--
	A1	10329.982	--
	t1	1938.8986	1.98769

Fig. S29. The decay curve of ground sample of **1**·4CH_2Cl_2.

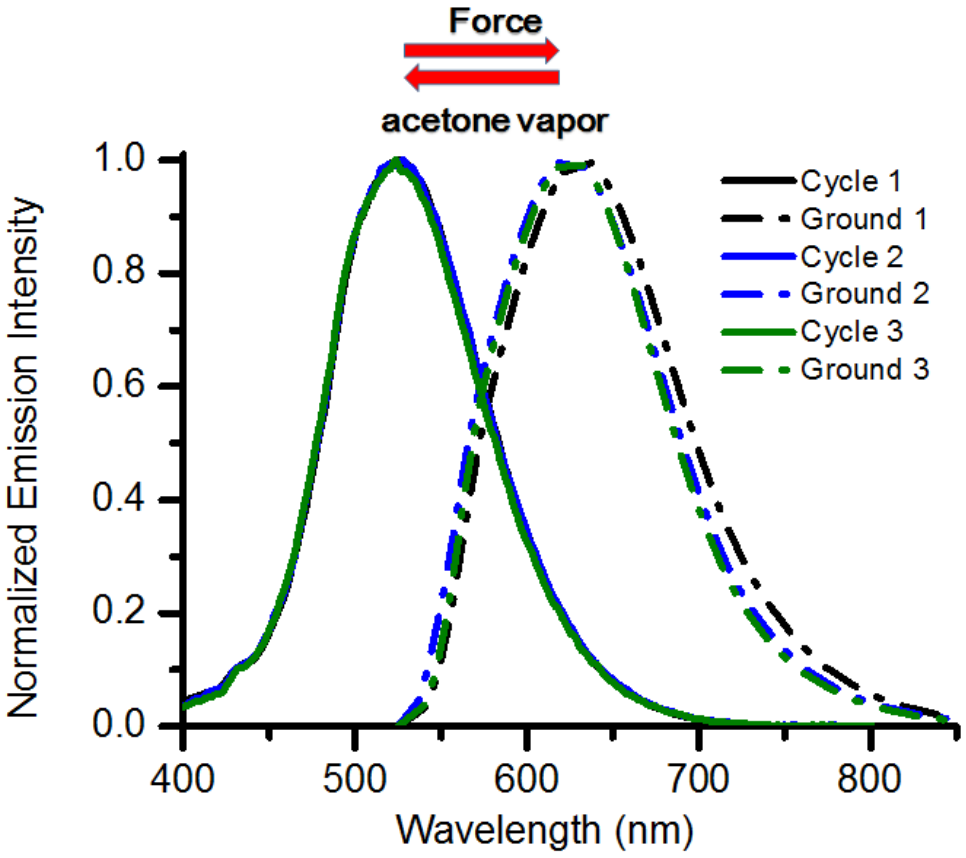

Fig. S30. The emission spectra of PMMA film doped with 3% complex **1** for three pressing-restoring cycles.